Check for updates

NUCLEIC ACID THERAPEUTICS
Volume 00, Number 00, 2026
Mary Ann Liebert, A Part of Sage
© The Author(s)
DOI: 10.1177/21593337261494829

Antisense Oligonucleotides that Are Toxic to Prion-Infected Mice Share an Emergent Mechanism

Hien T. Zhao,[1] Jill O'Moore,[2] Daniel A. Sprague,[3] Juliana E. Gentile,[3] Sagar Damle,[1,*] Briana Noble,[1] Taylor L. Corridon,[3] Simone Lord,[3] Jason Le,[4] Samantha Graffam,[4] Michael Howard,[4] Kendrick DeSouza-Lenz,[4] Hongda Li,[1] John Matson,[1] Susan Li,[1] Stephanie Klein,[1] Tyler Caron,[4] Alissa A. Coffey,[3] Sonia M. Vallabh,[3,5–7] Holly B. Kordasiewicz,[1] Andrea Grindeland Panter,[2] and Eric Vallabh Minikel[3,5–7]

Some, but not all, gapmer antisense oligonucleotides (ASOs) delivered into cerebrospinal fluid exhibit fatal subacute toxicity in late-stage prion-infected mice but not in uninfected mice. Here, we performed a battery of *in vivo* studies demonstrating that the toxicity is compound- and disease- stage-dependent, and not predicted by behavioral or molecular measurements in uninfected animals. A panel of toxic ASOs all elicited a consistent transcriptomic response signature in prion-infected mice, which emerged over the course of 7 days post dose. This signature, driven chiefly by decreased expression of a specific set of astrocyte-expressed genes, was absent in uninfected mice receiving the same ASOs, was absent, less intense, and/or more transient in infected mice receiving tolerated ASOs, and was distinct from the transcriptomic effect of prion disease itself. Our data argue that the toxicity is an interaction between ASO and prion disease at high doses for specific compounds, and does not represent an exacerbation of ASO toxicity nor of prion disease.

Keywords: antisense oligonucleotide, toxicology, prion, transcriptomics

Introduction

Oligonucleotide drugs including RNAse H1 antisense oligonucleotides (ASOs) are being evaluated for their ability to lower PrP expression as a therapeutic strategy in prion disease.[1–3]

In studies of ASOs administered intracerebroventricularly (ICV) to prion-infected mice at 60–120 days postinoculation (dpi), we and others have sometimes observed a fatal subacute toxicity, with rapid decline requiring euthanasia within ~1–4 weeks postdose.[1,2,4] The same ASOs at the same dose levels were tolerated in uninfected mice or in mice at early stages of prion infection. This is not an on-target effect, because it was sometimes observed for a control ASO not targeting PrP,[1] but little else is known about the toxic mechanism.

ASO toxicology has been studied extensively in the liver, where delocalization of paraspeckle proteins to nucleoli[5] and off-target cleavage of long transcripts[6–9] have been identified as toxic mechanisms for certain compounds, and sequence features including guanine content have been identified as predictors of toxicity.[10–12] In the Central Nervous System (CNS), acute ASO toxicity (within 3 hours of dosing) has been linked to high phosphorothioate and guanine content[13,14] and to divalent cation chelation,[14–17] but scant data have been published regarding mechanisms of delayed ASO toxicity in the CNS. In our effort to understand the mechanism of prion disease-specific toxicity of ASOs, we therefore employed a wide variety of techniques in a battery of *in vivo* studies. We identified a unique transcriptomic signature of ASOs toxic in prion-infected mice that is distinct from the transcriptomic signature of prion disease itself and is not elicited by the same ASOs in naive mice.

Methods

Animals and ethical approvals

All rodent studies were conducted under approved Institutional Animal Care and Use Committee (IACUC) protocols: Broad Institute protocol 0162-05-17, Ionis Pharmaceuticals protocols 2021-1176 (mice) 2021-1164 (rats), and McLaughlin

[1]Ionis Pharmaceuticals, Carlsbad, California, USA.
[2]Weissman Hood Institute, Great Falls, Montana, USA.
[3]Program in Brain Health, Broad Institute of MIT and Harvard, Cambridge, Massachusetts, USA.
[4]Comparative Medicine, Broad Institute of MIT and Harvard, Cambridge, Massachusetts, USA.
[5]McCance Center for Brain Health and Department of Neurology, Massachusetts General Hospital, Boston, Massachusetts, USA.
[6]Department of Neurology, Harvard Medical School, Boston, Massachusetts, USA.
[7]Prion Alliance, Cambridge, Massachusetts, USA.
*Present address: Eli Lilly, Indianapolis, IN 46285 USA.

Research Institute protocol 2023-AG-77. Wild-type (WT) mice were C57BL/6N females purchased from Taconic Biosciences 4–10 weeks old at inoculation for prion-infected cohorts and 8–12 weeks old at first ICV injection for uninfected cohorts. Alexander disease (AxD) mice have been previously described;[18] these studies used mixed sex cohorts. Rat studies used Sprague-Dawley females obtained from Harlan Laboratories (stock # 213 M, Livermore, CA), 8–12 weeks at first IT injection. Animals were group-housed with food and water provided *ad libitum*.

Prion inoculation and animal monitoring

Mouse prion inoculations were performed as previously described.[2] Briefly, the RML prion strain[19] was used, 30 μL of a 1% brain homogenate in PBS was freehand inoculated into the brain of anesthetized animals using a 31G insulin syringe. Prion-inoculated animals were weighed at least weekly from the time of first ICV ASO administration or 120 dpi, whichever came first, and were CO_2 euthanized at 20% body weight loss relative to a baseline taken at 16 weeks of age, or, if moribund, defined as unable to reach food or water. All causes of death are included in survival curves. Mice were euthanized by CO_2 asphyxiation.

Drug formulation

ASOs were formulated as described previously[2] in dPBS (Gibco 14190) without added magnesium or calcium. Divalent siRNA was formulated as described previously,[3] with Ca2+: Mg2+:divalent siRNA in a 14:2:1 molar ratio, in aCSF (137 mM NaCl, 5 mM KCl, 20 mM D-glucose, and 8 mM HEPES).

ICV drug administration in mice

ICV administration in mice was performed as previously described.[2,3,20] Briefly, isoflurane-anesthetized mice were immobilized in a stereotactic apparatus (ASI Instruments, SAS-4100) with 18° ear bars and the mouse adapter tooth bar set to −8 mm to level the bregma and lambda. A ∼1 cm midline scalp incision was made, and the periosteum was scraped from the skull with a sterile cotton-tipped applicator to expose bregma. A 10 μL microsyringe (Hamilton 80065) fitted with a 26G Huber point needle was used for ASO administration while a 10 μL microsyringe (Hamilton 80308) fitted with a 26G curved, beveled needle was used for siRNA administration. From bregma, the needle was moved 0.3 mm rostral, 1.0 mm right, and 3.0 mm downward past the skull. The indicated ASO doses were injected over ∼10 s in a 10 μL volume in dPBS (Gibco 14190), and the needle was left in place for 3 min before being slowly withdrawn under gentle downward pressure on the skull. The siRNA doses were delivered bilaterally at the above coordinates, administering 5 μL per side for a total injection volume of 10 μL, formulated as described previously.[3] Incisions were closed with a horizontal mattress stitch (Ethicon 661H), and animals recovered from anesthesia on a warming pad in their home cages.

Intrathecal drug administration in rats

Intrathecal (IT) dosing in rats was performed following the procedure previously described.[21] Briefly, rats were isoflurane anesthetized and the lumbar IT space was catheterized. For each animal, test article (ASO or vehicle) was injected at a 30 μL volume into the subarachnoid space via the catheter over approximately 30 seconds, followed by a 40 μL vehicle flush to clear the catheter dead volume. Immediately following dosing, animals were returned to their home cages with clean bedding to recover from anesthesia.

Monitoring endpoints in uninfected animals

Functional observational battery (FOB) scoring was performed as described[13] for mice and rats at 3 hours post-dose and every other week until up to 8 weeks post-dose.

RT-qPCR for inflammatory markers

Inflammatory markers (*Aif1*, *Cd68*, *Gfap*) were measured in a ∼5 mg piece of cortex caudal to the injection site, and in a 3 mm segment of thoracic spinal cord. These samples were homogenized in 500 ul of RLT buffer using the RNeasy 96 purification kit (Qiagen, Valencia, CA) containing 1% 2-mercaptoethanol. RNA was isolated from 30 uL of lysate using 96-well filter plates and chaotropic salts (Pall Life Sciences, Ann Arbor, MI). RT-qPCR was performed using StepOne Plus Realtime PCR instruments (Applied Biosystems, Carlsbad, CA). Briefly, 20 μL RT-PCR reactions containing 5 μL of RNA were run with 5′Fam, 3′Tamra using the primer/probe-sets listed below. All RT-qPCR reactions were run in triplicate. Values from the respective transcripts of interest (*Aif1*, *Cd68*, or *Gfap*) were normalized to the housekeeping gene *Ppia*, and further normalized to vehicle (PBS) group. Primers and probes were as follows. *Ppia* forward: TCGCCGCTTGCTGCA, reverse: ATCGGCCGTGATGTCGA, probe: CCATGGTCAACCCCACCGTGTTC. *Aif1* forward: TGGTCCCCCAGCCAAGA, reverse: CCCACCGTGTGACATCCA, probe: AGCTATCTCCGAGCTGCCCTGATTGG. *Cd68* forward: TGG CGGTGGAATACAATGTG, reverse: GATGAATTCTGCGCCATGAA, probe: CCTTCCCACAGGCAGCACAGTGG. *Gfap* forward: GAAACCAGCCTGGACACCAA, reverse: TCCACAGTCTTTACCACGATGTTC, probe: TCCGTGTCAGAAGGCCACCTCAAGA.

RT-qPCR for target engagement

To measure enhanced divalent siRNA potency, including in the prion-infected model, RNA was isolated from whole mouse brain hemispheres including cerebellum, using the AllPrep DNA/RNA mini kit (Qiagen, 80204). Hemispheres were put in 3 mL RLT plus buffer containing 40 mM DTT and homogenized using 1.4 mm zirconium oxide beads in 7 mL screw-cap tubes (CK14 soft tissue homogenizing kit, Precellys KT039611307.7) by means of 3 × 40-s pulses on high in a Minilys homogenizer (Bertin EQ06404-200-RD000.0). RNA was isolated from 500 μL lysate and was finally eluted in a total volume of 100 μL RNase-free water. RT-qPCR reactions were prepared using 2 μL of purified RNA, TaqMan 1-step qRT-PCR master mix and TaqMan gene expression assays for mouse Tbp (Invitrogen, cat no.: Mm00446971_m) and mouse Prnp (Invitrogen, cat no.: Mm00448389_m1) in a 20 μL reaction volume. Here, RT-qPCR was run on a QuantStudio 7 Flex system (Applied Biosystems) in a MicroAmp Optical 384-well reaction plate (Applied Biosystems, cat no.: 4309849) using the following cycling conditions: reverse transcription 50C, 5 min; reverse transcription inactivation/initial denaturation 95°C, 20 s;

amplification 95°C, 3 s, 60°C, 30 s, 40 cycles. Each biological sample was run in duplicate, and the level of *Prnp* was first normalized to the housekeeping gene *Tbp* and then to undosed animals in the respective condition. Measurement of target engagement in the ASO 6 experiment utilized procedures similar to those for the inflammatory markers above, but with a whole brain hemisphere input and with the following primers/probes. *Prnp* forward: TCAGTCATCATGGCGAACCTT, reverse: AGGCCGACATCAGTCCACAT, probe: CTACTGGCTGCTGGCCCTCTTTGTGAC.

Immunohistochemistry (IHC) scoring

The tissues were formalin-fixed and then processed on a Sakura Tissue Tek tissue processor. After embedding, tissues were cut at 4 microns, air-dried overnight, and then dried at 60° for 1 h. Tissues sections were stained with either rabbit polyclonal antibodies against Iba1 (Fujifilm Wako, 019-19741), against ASO (Ionis in-house reagent[22]) or against glial fibrillary acidic protein (GFAP) (Dako, Z033401-2) and rabbit monoclonal antibodies against Calbindin (Abcam, ab108404) or against Prion protein (PrP) [EP1802Y] (Abcam, ab52604) on a Ventana Ultra staining system. For Iba1, Calbindin and PrP protein IHC, slides were treated with Heat-Induced Antigen Retrieval (HIER) using Ventana CC1 solution (Ventana, 950-500) for 64 min. For GFAP IHC, slides were treated enzymatically with Protease 2 (Ventana, 760-2019) for ASO IHC trypsin (Sigma, T8003) enzyme was used. In addition, slides for GFAP, ASO and PrP IHC were blocked with Endogenous Biotin Blocking Kit (Ventana, 760-050) and Normal Goat Serum (Jackson Immuno Labs, 005-000-121) before all primary antibodies were diluted with Discovery Antibody Diluent (Ventana, 760-108) and incubated for 1 h at 37°C. GFAP, ASO and PrP antibodies were detected with biotin-labeled goat anti-rabbit secondary antibody (Jackson Immuno Labs, 111-005-003) and the secondary antibody labeled with DABMap Kit (Ventana, 760-124). The antibodies against Iba1 and Calbindin were detected with UltraMap anti-Rabbit Polymer detection (Ventana, 760-4315). The rabbit polymer was then labeled with Ventana ChromoMap DAB kit (Ventana, 760-159). Images were scanned on a Hamamatsu S360 scanner at 20× resolution and scored by a board-certified histopathologist. Cellular ASO uptake and parenchymal/cellular PrP accumulation were assessed using a semi-quantitative scoring system. Cellular ASO uptake was scored 0 for no uptake, 1 for individual punctate stain within cytoplasm filling <10% per cell, 2 for up to 50% of cytoplasm filled, and 3 for >50% filled. PrP protein accumulation was scored 0 for no visible protein deposits, 1 for light brown stain intensity restricted to a few key brain areas, 2 for mild brown stain intensity in about 20%–30% of key areas and 3 for dark brown intense stain in most or all key areas such as cortex, hippocampus, cerebellum and thalamus. Scores of 0–3 were given on severity of gliosis and astrocytosis with 0–1 being unremarkable/similar to vehicle treatment, and 2–3 representing mild-moderate gliosis/astrocytosis. Calbindin score was either "yes" (1) for any calbindin loss in cerebellar Purkinje cell layer and their axons/dendrites and "no" (0) for no loss.

BJAB cell CCL22 induction assay

Innate immune activation potential via the TLR9 pathway was assessed in BJAB cells (DSMZ #ACC757), a human Burkitt lymphoma B-cell line with constitutive TLR9 expression, using the assay developed by Pollak et al.[23] Briefly, BJAB cells were cultured in RPMI supplemented with 20% FBS at 37°C in 5% CO_2 and plated in 96-well V-bottom plates at 7.5×10^5 cells/mL (50 μL per well). ASOs were then added by free uptake using 10 × dosing solutions, mixed briefly, and incubated for approximately 24 h. After treatment, cells were lysed and total RNA was extracted using the RNeasy Mini Kit (Qiagen) according to the manufacturer's protocol. CCL22 mRNA induction was measured as the primary readout of TLR9-mediated innate immune activation by one-step RT-qPCR in triplicate using TaqMan primer-probe sets (forward: CGCGTGGTGAAACACTTCTA; reverse: GATCGGCACAGATCTCCTTATC; probe: TGGCGTGGTGTTGCTAACCTTCA). Expression was normalized to total RNA quantified in duplicate using the RiboGreen assay (Life Technologies) and expressed as fold change relative to untreated controls (UTCs). Benchmark phosphorothioate oligonucleotides of known inflammatory potential (eg, ISIS 104838 as a minimally inflammatory control and ISIS 353512 or ODN2006 as positive controls) were included on each plate.

Pharmacokinetics

Oligonucleotide tissue concentrations were quantified in CNS tissue as previously described.[24] Briefly, frozen tissue samples (cortex) were homogenized in homogenization buffer (20 mM Tris pH 8.0, 20 mM ethylenediaminetetraacetic acid [EDTA], 0.1M NaCl, 0.5% NP-40) with lysing matrix beads (Matrix Green, Bio 101 No. 6040-801). They were run by ion-pairing liquid chromatography-tandem mass spectrometry (LC-MS/MS) on an Agilent 6460 triple quadrupole system (Agilent, Wilmington, DE, USA), using an ACQUITY UPLC OST C18 column (Waters, Milford, MA, USA) heated to 55°C with a flow rate of 0.3 mL/minute. A binary solvent system with mobile phase A (400 mM/L HFIP/15 mM/L TEA) and mobile phase B (MeOH) was used. A gradient from 10% to 40% MeOH over 6 min was used to elute the target analyte and internal standard. All mass measurements were acquired using MRM, with a precursor ion unique to the specific analyte and with a product ion of 94.8 for all transitions, including both the analyte and the internal standard (ISIS 764073). Mass spectra were obtained using a spray voltage of −1500 V, a nebulizer gas flow of 25 psig, a sheath gas flow rate of 12 L/min at 350°C, a drying gas flow rate of 5 L/min at 350°C, and a capillary voltage of −3750 V. Chromatograms were integrated and quantified using Agilent MassHunter software against the calibration curve of known ASO concentrations. Concentrations of each analyte were quantitated from its calibration curve, which had a quantitation range of 0.25–10 μM (approximately 0.2–70 μg/g, considering different molecular weight).

3′ seq transcriptomics

Sequencing and bioinformatics analysis were performed as described.[25] Briefly, libraries were constructed using the 3′QuantSeq FWD kit (Lexogen, Cat: #015.2 × 96) with custom first-strand synthesis primers. Reverse transcription was performed using QuantaBio qScript reverse transcriptase. Sequencing was conducted on an Illumina NovaSeq platform

at a depth of 5–10 million reads per sample. After aligning reads to mus-musculus 109 genome, gene assignments were performed with FeatureCounts. Unique molecular identifiers (UMIs) were used to remove PCR duplicates via umi_tools (version 1.1), discarding reads mapping to the same gene with identical 12 nt UMIs. Post-deduplication, unique reads were quantified using Salmon[26] (version 0.7.2) in pseudoalignment mode with default parameters, leveraging gene models from Ensembl Mouse Transcriptome Build 109. Gene expression was calculated in transcripts per million (TPM), obtained by normalizing gene-specific read counts by the total number of mapped unique reads (in millions). Library duplication rates ranged from 60% to 80%, and 1–3 million unique reads were captured per sample. Differentially expressed (DE)-gene expression analysis was conducted per sample on gene counts using DESeq2[27] with standard parameters. Genes with an adjusted *P*-value of significance < 0.05 were identified as DE and selected for comparisons. To ensure robust analysis, only genes expressed above 2.5 TPM in UTCs were included. This threshold, equivalent to approximately five counts per gene at typical sequencing depth, limits the analysis to genes that are most reproducible.

Cell type assignment

DE genes were assigned to enriched cell types based on previously reported single nucleus transcriptomic data.[28] Loupe Browser v8 was used to analyze mouse cortex single nucleus transcriptomes and compute differential gene expression (DGE) of each cell type of interest (astrocytes, microglia, oligodendrocytes) compared to all other cell types in the mouse cortex. Genes were considered to be enriched in a cell type if they had a mean expression ≥ 1 log2 UMI (unique molecular identifier) count per nucleus in that cell type as well as a log2 fold change ≥2 and nominal *P* value < 0.01 versus all other cell types.

Use of large language models

Claude Code (Sonnet 5) was used to generate some of the source code for this study. Code was then tested and validated by DAS and/or EVM.

Results

For *in vivo* evaluation, we selected a total of 21 ASOs including 6 previously reported[1,2,29] compounds targeting mouse *Prnp*, 2 previously reported nontargeting controls,[1,2] 4 gap modifications of one of the *Prnp* compounds, and 9 compounds directed against other human genes, with no target in the mouse genome, spanning a range of lengths, chemical configurations, and sequence compositions (Table 1).

ASO 2 at 300 μg single ICV dose was previously observed to result in subacute toxicity when administered at 120 days post-inoculation (dpi)[1] in WT mice intracerebrally infected with the Rocky Mountain Laboratories (RML) prion strain,[19] a standard *in vivo* prion challenge model. We sought to test whether prion disease stage-dependent toxicity occurs at lower doses. In a dose-response experiment with ASO 2 administered at 90 dpi (Fig. 1A), ASO 2 exhibited toxicity only at 300 μg, resulting in euthanasia of 4/4 animals at 6 days postdose (96 dpi). All other tested doses were tolerated and dose-dependently efficacious, increasing survival time from a median of 163 dpi in the PBS group to 171 dpi at 10 μg (+5%, $P = 0.88$, 2-sided log-rank test), 182 dpi at 30 μg (+12%, $P = 0.0067$), 191 dpi at 50 μg (+17%, $P = 0.0067$), or 220 dpi at 100 μg (+35%, $P = 0.0067$).

Table 1. ASOs Used in This Study

Name	*Target*	*Sequence and chemistry*	*Citation*
ASO 1	*Prnp*	**CT**o**A**o**T**TTAATGTC**A**o**G**o**TCT**	Ref[1]
ASO 2	*Prnp*	**TT**o**G**o**C**AATTCTAT**C**o**C**o**AAA**	Ref[1]
ASO 2 + 2'OMe gap position 2	*Prnp*	**TT**o**G**o**C**AATTCTAT**C**o**C**o**AAA**	This study
ASO 2 + full 2'MOE	*Prnp*	**TT**o**G**o**CAATTCTAT**C**o**C**o**AAA**	This study
ASO 2 + MsPA (design 1)	*Prnp*	**TT**o**G**o**C**AμAμTμTCTAT**C**o**C**o**AAA**	This study
ASO 2 + MsPA (design 2)	*Prnp*	**TT**μ**G**o**C**AμAμTTCTAT**C**o**C**o**AAA**	This study
ASO 3	*None*	**CG**o**C**o**T**ATACTAATC**A**o**TAT**	Ref[1]
ASO 4	*None*	**CC**o**T**o**A**o**T**AGGACTATCC**A**o**G**o**G**o**AA**	Ref[2]
ASO 5	*Prnp*	**TT**o**G**o**C**o**A**ATTCTATCCA**A**o**A**o**TAA**	Ref[2]
ASO 6	*Prnp*	**CT**o**T**o**C**o**T**ATTTAATGTC**A**o**G**o**TCT**	Ref[2]
ASO 7	*Prnp*	**TA**o**G**o**C**o**C**TTTGTACCTT**A**o**A**o**CCA**	Ref[29]
ASO 8	*Prnp*	**GC**o**C**o**A**AGGTTCGC**C**o**A**o**TGA**	Ref[29]
ASO A	*LRRK2*	**AT**o**G**o**T**o**T**CATATCCTTT**A**o**A**o**CCC**	Ref[30]
ASO B	*LRRK2*	**AT**o**T**o**T**o**T**oGAATTACAAT**G**o**C**o**GGT**	Ref[30]
ASO C	*ATXN3*	**TC**o**A**o**C**o**C**ACAAACTCAT**G**o**G**o**ACT**	This study
ASO D	*ATXN2*	**AC**o**C**o**C**o**T**TTCCATGTGA**A**o**C**o**ATT**	This study
ASO E	*ATXN2*	**CA**o**T**o**T**o**T**oTGAATTACAA**T**o**G**o**CGG**	This study
ASO F	*ATXN3*	**AT**o**GTT**AATACTTTTT**CC**o**AGC**	This study
ASO G	*ATXN2*	**GC**o**A**o**A**o**A**oGACTTTGAAA**T**o**C**o**TCA**	This study
ASO H	*ATXN2*	**AG**o**T**o**G**o**C**TATAATTCTT**G**o**C**o**TTC**	This study
ASO I	*ATXN2*	**GT**o**G**o**G**o**C**oTTTAAAAACT**A**o**G**o**GTA**	This study

Code for ASO chemical modifications is as follows. Nucleotides: default = unmodified deoxyribose (2′H; DNA); **bold** = 2′ methoxyethyl (MOE); underline = 2′–4′ constrained ethyl (cET), *italic* = 2′-O-methyl. Backbone linkages: default = phosphorothioate (PS); o = phosphodiester (PO); μ = mesyl phosphoramidate (MsPA). All C are 5-methylcytosine.

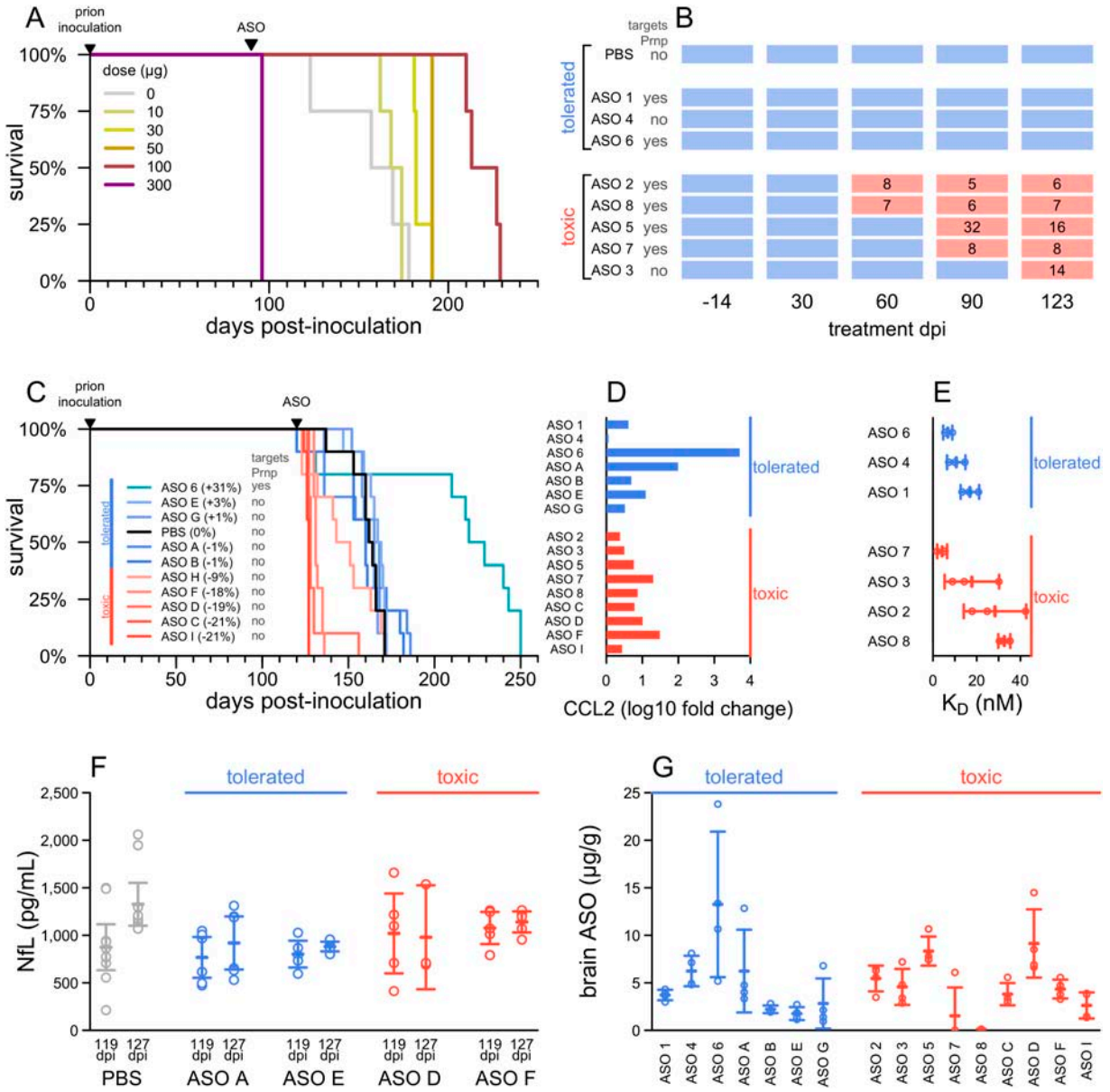


FIG. 1. Prion disease-specific toxicity is ASO-specific, dose-dependent, disease stage-dependent, target-independent, and not predicted by neurofilament, pharmacokinetics, or innate immune stimulation. **(A)** Dose-response survival study of ASO 2 at 90 dpi. $N = 4$ mice per group. **(B)** Time series administration of ASOs indicated on y axis to groups of $N = 4$ RML prion-infected mice at dpi timepoints indicated on x axis. Blue = tolerated, mice harvested at 150 dpi. Orange = toxic, mice harvested at the number of days post-dose indicated in the number printed on the rectangle. These data were previously included in a dissertation.[31] **(C)** Survival study of PBS, ASO 6, and ASOs A through H ($N = 10$ per group) at 300 µg in RML prion-infected mice at 120 dpi. Indicated in the legend are the percent change in mean survival time relative to PBS for each ASO, and whether the ASO targets Prnp. **(D)** BJAB cells CCL22 induction (log10 fold changes); see Methods for details. **(E)** Previously reported binding affinity (K_D) values[29] measured by isothermal titration calorimetry for recombinant PrP, reproduced here for comparison to toxic/tolerated status based on the 123 dpi timepoint of the experiment in panel B. Points are replicates, segments and error bars are means and 95% confidence intervals. **(F)** Plasma NfL at 119 dpi (1 day pre-dose) and 127 dpi (7 days post-dose) in a subset of the animals from panel C, $N = 10$ per group for PBS, $N = 3$–6 per group for other ASOs. **(G)** Drug concentration in whole brain hemispheres (µg drug per g of brain tissue) at 7 days post 300 µg dose in naive animals. $N = 4$ per group. ASO, antisense oligonucleotide; RML, Rocky Mountain Laboratories.

We also sought to test the disease stage dependence of the toxicity phenomenon. In a separate study, groups of $N = 4$ RML prion-infected WT mice received PBS or 300 µg of any of ASOs 1–8 (including *Prnp*-targeting and non-*Prnp* targeting) at a range of timepoints from −14 (meaning 14 days before prion infection) to 123 dpi (Fig. 1B) and were monitored for sudden decline. ASOs 1, 4, and 6 were tolerated at all timepoints tested. The remaining ASOs exhibited toxicity beginning at different disease stages: ASO 3 became toxic only at 123 dpi, while ASOs 2 and 8 were already toxic at 60 dpi. No ASOs were toxic earlier than 60 dpi, approximately the time in disease when CNS GFAP and

plasma neurofilament light (NfL), markers of neuroinflammation and neuronal damage, begin to be elevated in the RML-infected challenge model.[2,32] There was no obvious correlation between the disease stage required for toxicity and the number of days between drug administration and sudden decline. Immunohistochemical analysis revealed no obvious differences in ASO uptake, PrP knockdown, or neuroinflammatory response as indicated by GFAP or IBA1 staining, between toxic versus tolerated ASOs (Supplementary Fig. S1). When 7 of these ASOs were also tested in a closely monitored 4-week study at 500 μg at 120 dpi, no compound exhibited perfect tolerability (and even 2/6 PBS animals died) but ASOs 1, 4, and 6 were replicated as relatively well-tolerated compounds (Supplementary Table S1). Close observation of the mice that experienced toxicity revealed hindlimb weakness progressing rapidly to paralysis within 24 h, requiring euthanasia.

We compared ASO 6, the best-tolerated *Prnp*-targeting compound, against 9 control ASOs not directed against *Prnp* in a survival study in RML prion-infected WT mice with a single 300 μg dose at 120 dpi (Fig. 1C). ASO 6 was effective, resulting in a survival time increase from 161 ± 10 dpi (mean ± SD) for PBS to 211 ± 47 dpi (+31%, $P = 2.2e\text{-}4$). Of the remaining ASOs, 4/9 exhibited mean survival equivalent to PBS (±3%) and were classified as tolerated, while 5/9 resulted in numerically foreshortened lifespan, with mean death 6 to 27 days postdose, corresponding to a change in survival of −9% to −21% relative to PBS, and were classified as toxic. These data were concordant with previous work demonstrating the benefit of PrP lowering in prion disease, while recapitulating the toxicity of certain ASOs in prion disease RML mouse model, which is not due to on-target PrP lowering.[1,2]

Armed with a panel of ASOs classified as toxic or tolerated in these RML prion model survival studies, we sought to identify measurable biomarkers, predictors, or classifiers of prion disease-dependent toxicity. First, as certain ASOs have been shown to activate innate immune responses, which we hypothesize could underlie the toxic versus tolerated ASOs identified in RML prion model, we evaluated these ASOs in the BJAB assay by measuring fold CCL22 transcript induction following ASO treatment.[23] This assay had been shown[23] to differentiate ASOs that activate innate immunity via TLR9 signaling versus those that do not. CCL22 transcript induction following ASO treatment was not higher for toxic than tolerated ASOs (Fig. 1D), arguing against a role for ASO-specific immune activation in this toxicity phenomenon. Another factor contributing to the toxicity observed could be preferential binding of toxic ASOs to PrP vs tolerated ASOs. Our previous work measuring binding affinities of the same panel of toxic versus tolerated ASOs[29] for recombinant PrP showed similar binding affinities, arguing against an aptameric effect (Fig. 1E). Next, we reasoned that toxic ASOs could result in more accelerated damage as measured by plasma NfL levels, a commonly used marker of neuronal damage.[33] Therefore, we selected two toxic ASOs D and F and two tolerated ASOs A and E and measured plasma NfL at 119 dpi in RML model (the day before ASO administration) and at 127 dpi (7 days post-ASO administration). In PBS-treated RML-infected animals over this 8-day period, mean plasma NfL increased +52% (874 pg/mL to 1326 pg/mL), consistent with disease progression (though the effect of ICV surgery cannot be entirely ruled out). There was no difference in plasma NfL trajectory between the toxic versus tolerated ASOs; however (Fig. 1F), even though at 127 dpi, animals treated with ASOs D and F were only 4 and 5 days, respectively, from their expected mean survival (Fig. 1C). Next, we hypothesized that a sequence-specific difference in ASO uptake and/or tissue residence could contribute to the observed toxicity phenomenon. Due to the infectious nature of RML-infected tissues, and the safety requirement necessary to analyze such samples, we opted to measure brain drug concentration at 7 days after a single 500 μg ICV dose in naive WT mice from similar age, gender and source of the WT mice inoculated with RML prions. While this may not fully reflect the extent of drug uptake and accumulation in the RML model, the concentrations measured may be sufficient to differentiate those sequences that are high versus low accumulating. While the data demonstrated pharmacokinetic differences across the ASOs evaluated, they did not show a pharmacokinetic difference between toxic versus tolerated ASOs (Fig. 1G). Across seven additional *in vivo* studies in uninfected mice and rats, we also measured a battery of inflammatory qPCR markers (Aif1, Gfap, Cd68), immunohistochemistry (IHC) scores (IBA1 and Calbindin), and FOB behavioral scores post-drug administration acutely and up to 8-weeks post dosing, for a total of 42 quantified endpoints, none of which discriminated toxic from tolerated ASOs (Supplementary Fig. S2).

The foregoing results suggested that the subacute toxicity phenomenon is highly prion disease-specific and unlikely to be predicted by tolerability assays or other measurements in uninfected animals. We therefore sought to understand the mechanism more deeply by studying the molecular effects of toxic ASOs on prion-infected animals. We performed bulk transcriptomics on whole brain hemispheres of mice inoculated with RML prions or control brain homogenate (CBH) and treated with 300 μg of a panel of toxic and tolerated ASOs, at 120 dpi and harvested at 127 dpi. Projection of transcriptomes onto 2 dimensions showed a clear clustering of RML versus CBH brains, and an emerging toxic ASO clustering only in RML—but not CBH-inoculated brains (Fig. 2A). Specifically, among RML-infected brains, there were two distinct clusters of toxic versus tolerated ASOs, while toxic ASO-treated CBH mice clustered with PBS-treated CBH mice. Among RML-infected mice, the DGE signature of toxic ASOs versus PBS prominently featured downregulation of a larger number of astrocyte-specific genes (Fig. 2B). From this DGE signature we selected the $N = 65$ genes with adjusted P value < 0.05, base mean (mean expression in PBS animals) of >10 TPM, and a ≥2-fold increase or decrease in expression. These 65 genes were then used to compute a toxicity score (tox score) for each individual ASO when compared to PBS, defined as the sum of the log2 fold change of each gene times their expected sign (meaning that genes count toward the score when they change in the expected toxic direction, and count against the score if they move in the opposite direction). Tox scores were high (range 31–66) for 5/5 individual toxic ASOs in RML-infected mice, which is expected since the score was based on these ASOs. Tox scores were low (range 2 to 17) for 4/4 tolerated ASOs in RML-infected mice, which were

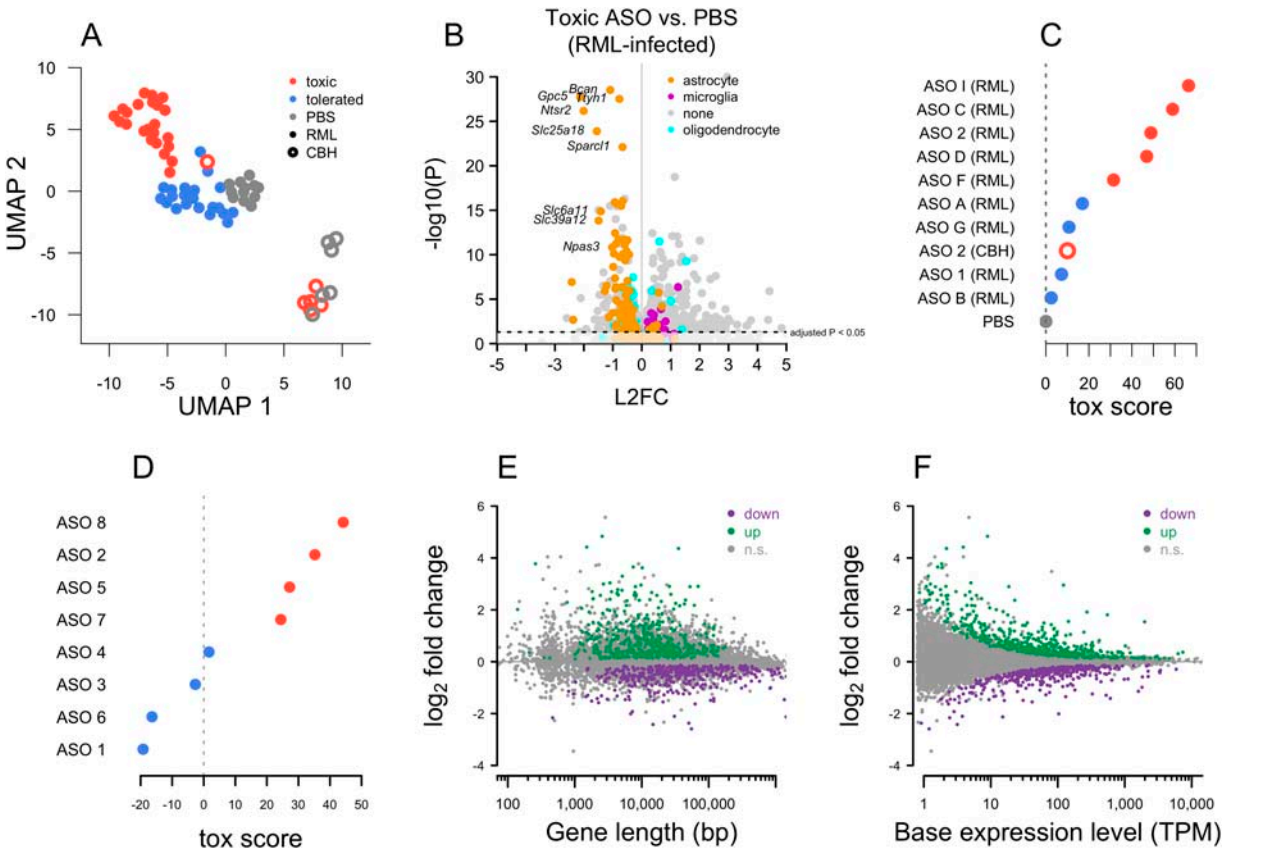


FIG. 2. Transcriptomic signature of toxic vs tolerated ASOs in noninfected vs prion-infected mice. **(A)** Uniform Manifold Approximation and Projection (UMAP)[34] of whole transcriptomes onto 2-dimensional space. Each point 1 is mouse. Colors indicate the classification of each ASO according to its tolerability (toxic vs. tolerated) at 300 μg in 120 dpi RML prion-infected mice in Figure 1C. Solid symbols are RML prion-infected mice, hollow symbols are uninfected mice receiving the same ASOs. The one CBH animal (hollow orange symbol) that clusters with the RML animals is suspected to be a sample swap, though after careful review of records no evidence of a swap was found. **(B)** Volcano plot of differential gene expression (DGE) of all prion-infected mice receiving toxic ASOs in panel A ($N = 6$ per group), versus prion-infected mice receiving PBS in panel A ($N = 12$). Each point is one gene. Transcripts are colored by their expression enrichment in select cell types, see Methods for details. The dashed line indicates a multiple testing-corrected P value of 0.05. The x-axis is log2 fold change. **(C)** Tox scores calculated from the DGE profile of each ASO indicated on the y-axis (all in prion-infected animals except for the hollow symbol representing ASO 2 (CBH), which refers to uninfected (CBH-inoculated) animals; $N = 6$ per group, versus PBS ($N = 12$). Each point is one group. **(D)** Tox scores from the animals treated with the toxic vs. tolerated ASOs at 90 dpi in Figure 1B, versus PBS controls (all $N = 4$ per group). Each point is one group. Note that toxic ASO-treated RML-infected animals were harvested upon observation of toxicity at the days post-ASO dosing indicated in Figure 1B, while tolerated ASO- and PBS-treated RML-infected animals were harvested at 150 dpi, thus their disease stages are not all the same, hence their use as a confirmatory rather than discovery cohort here. **(E)** Transcript length versus differential expression. Each point is one gene. Colored points have adjusted P values < 0.05, while gray points are nonsignificant. Positive y-axis positions indicate genes that go up in the toxic ASO-treated RML animals, while negative y-axis positions indicate genes that go down in the toxic ASO-treated RML animals. **(F)** As in **(E)** but for basal expression level (base mean transcripts per million or TPM, in PBS mice). TPM, transcripts per million.

not involved in generation of the score. The tox score for ASO 2 in CBH mice was also low (10), confirming that the transcriptomic signature is not observed in uninfected mice (Fig. 2C).

To further validate the applicability of the transcriptomic tox score, we calculated it for the panel of ASOs previously tested in the time-series study (Fig. 1B), which were not used to generate the list of tox score genes. 4/4 toxic ASOs that led to rapid decline within 5–32 days post dose at a 300 μg dose at 90 dpi in that study all had high positive tox scores (range 24–44), while 4/4 ASOs that were tolerated at 300 μg at 90 dpi and for which animals were therefore not harvested until 150 dpi, all exhibited low or negative tox scores (range −19 to 2) (Fig. 2D). The above results all pointed to transcriptomic signature of disease stage-dependent ASO toxicity in prion-infected animals, which is shared across many distinct ASOs, but is not observed when the same ASOs are dosed into naive, uninfected mice, and is also distinct from the transcriptomic signature of prion disease.

We next asked what the DE genes in this signature have in common. Because locked nucleic acid (LNA) toxicity in the liver is reported to be driven by promiscuous downregulation of highly expressed long transcripts,[6] we examined the effects of gene length and basal expression level. We found that our DGE signature showed no particular enrichment of downregulated long transcripts (Fig. 2E), nor were expressed

transcripts particularly skewed for direction of effect (Fig. 2F). RNase H1-dependent delocalization of paraspeckle proteins to nucleoli was previously reported to drive gapmer ASO toxicity in the liver,[5] but pathway analysis using Gene Set Enrichment Analysis (GSEA) did not identify any enrichment of reported nucleolar transcripts[35,36] nor of transcripts down-regulated by expression of a mutated form of the paraspeckle protein FUS[37] (Supplementary Fig. S3A). Pathway analysis using GSEA[38] identified enrichment of several pathways including ribosome-associated quality control and translation elongation, but none of these nominated specific mechanistic hypotheses (Supplementary Fig. S3B). Evaluations of gap modifications previously shown to improve therapeutic index in the liver[5,39] were inconclusive. One ASO with full 2'MOE modification, expected to abolish RNase H1 cleavage, remained toxic, while one ASO with a single 2'OMe gap modification elicited increased survival (Supplementary Fig. S4A-C). Differences in target engagement, limited pharmacokinetic characterization, and incomplete transcriptomic data, together with the small number of compounds examined, make it difficult to draw firm conclusions about mechanism or general design principles (see Discussion).

We also asked whether the transcriptomic tox signature might represent an exaggeration of the transcriptomic effects of underlying prion disease. To characterize the transcriptomic signature of the natural history of prion infection, we also harvested brains from untreated RML and CBH mice at 60 and 89 dpi and from PBS-treated RML and CBH mice at 120 and 149 dpi. The transcriptomic signature of prion disease (Fig. 3A–D) across these timepoints prominently featured the progressive upregulation of microglial and astrocytic genes, typified by markers *C1qa* and *Gfap*, which were the top two hits when RML and CBH mice were compared at 149 dpi (Fig. 3D). This was consistent with expectation based on prior work by Sorce & Nuvolone et al,[40] which we re-analyzed and compared to our data (Supplementary Fig. S5), revealing a highly similar transcriptomic signature of prion disease between the two studies.

In this same study, we also treated RML-infected or CBH-inoculated mice with 300 μg of ASO 1 (tolerated), 2 (toxic), or PBS at 90 dpi, and harvested brains for transcriptomics at 1, 4, and 7 days post-dose, as well as 30 days post-dose for ASO 1 (the other groups do not survive this long). We selected ASO 2 as the toxic ASO for this study because it was toxic as early as 60 dpi (Fig. 1B), consistently showed high tox scores (Fig. 2C–D), and, unlike ASO 8, showed good tolerability metrics by behavioral, immunohistochemical, and inflammatory marker readouts in naïve, uninfected

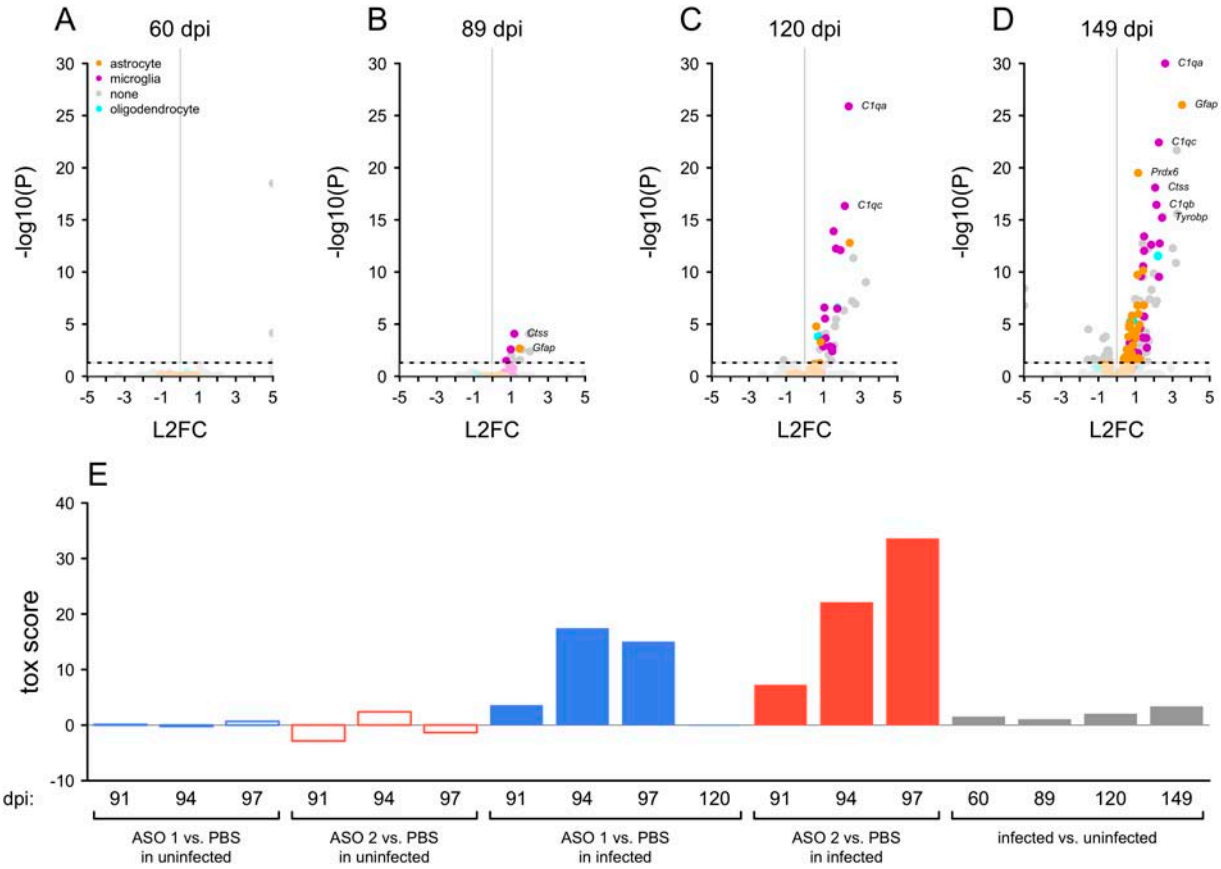


FIG. 3. The transcriptomic effect of prion disease is distinct from the tox signature. **(A–D)** Volcano plot of DGE in RML prion-infected mice versus uninfected mice at ($N = 4$ per group) at **(A)** 60 dpi, **(B)** 89 dpi, **(C)** 120 dpi, and **(D)** 149 dpi. Transcripts are colored by their expression enrichment in select cell types, see key in panel A. The dashed line indicates a multiple testing-corrected P value of 0.05. The x-axis is log2 fold change. **(E)** Tox scores for pairwise comparisons of groups of $N = 4$ mice indicated along the x-axis, colored by whether the ASO is classified as toxic or tolerated at 90 dpi according to the data from Figure 1B. Each bar is one group. Comparisons of prion-infected versus uninfected mice are shown in gray.

mice (Supplementary Fig. S2). We chose ASO 1 as the "tolerated" control because it has an identical chemical configuration as ASO 2, differing only in sequence (Table 1). We calculated the tox score for pairwise group comparisons in this study (Fig. 3E). Neither ASO 1 nor 2 in CBH mice showed any appreciable tox score at any timepoint. ASO 1, which is generally tolerated in prion-infected mice (Fig. 1B), though not perfectly so (Supplementary Table S1 and ref 2), had a tox score that rose somewhat between 1 and 7 days postdose, then declined by 30 days postdose. ASO 2 rose higher and more rapidly than ASO 1, reaching a score of >30 by 7 days postdose. Comparison of untreated (no ASO or PBS injection) prion-infected to uninfected mice did not yield a high tox score at any timepoint in disease. All of the above observations confirmed that the transcriptomic tox signature is highly distinct from the transcriptomic impact of prion disease.

Having recently observed deeper PrP knockdown using ASOs in RML-infected mice[41] and in spontaneously sick Tg (Vole) mice[42] than we typically observe in naive, uninfected animals, we asked whether ASOs might be differentially potent in prion-infected mice. We chose ASO 6 and a treatment timepoint of 105 dpi, because this ASO is sufficiently well-tolerated to support a 30-day target engagement study in the RML-infected model, and 135 dpi is a timepoint at which we expect all dosed animals to be surviving. We dosed RML-infected or uninfected WT mice at 105 dpi with 100 or 300 μg of ASO 6, and performed qPCR on whole brain hemisphere RNA at 30 days postdose. Knockdown was significantly deeper in RML-infected mice than in uninfected mice, with 26.6% versus 68.4% residual *Prnp* mRNA at 100 μg, a 41.8% difference (P = 1.6e-11) and 17.9% vs. 43.4% residual *Prnp* mRNA at 300 μg, a 25.5% difference (P = 1.3e-9; Fig. 4A). We asked whether this increased potency in RML-infected mice was unique to ASOs, or could also be observed for another oligonucleotide therapeutic. We tested 1682-s4, a divalent siRNA directed against mouse *Prnp*[3]. 1682-s4 likewise proved more potent in RML-infected mice, with 52.6% versus 88.7% residual *Prnp* mRNA at 70 μg, a 36.0% difference (P = 1.5e-4), and 34.8% versus 64.5% residual *Prnp* mRNA at 244 μg, a 29.7% difference (P = 2.2e-4; Fig. 4B). Because oligonucleotides must undergo endosomal escape to reach active subcellular compartments, we queried our transcriptomic data, and found that galectin 3, galectin 9, and galectin 3-binding protein, are transcriptionally upregulated in the later stages of prion disease (Supplementary Fig. S6; see Discussion). Of these 3 genes, only galectin 3 (*Lgals3*) is also among the 65 genes identified as part of the transcriptomic tox score, albeit with a more modest log2 fold change (1.39 in the tox score from Fig. 2B), versus 2.34 in RML versus CBH mice at 127 dpi (Supplementary Fig. S6A).

Discussion

Previously, we observed prion disease stage-dependent toxicity of some ASOs, irrespective of whether they target *Prnp*, when delivered into cerebrospinal fluid in late-stage prion-infected mice.[1,2,4] Here, we studied a large panel of ASOs and found that approximately half of them result in this same phenomenon. Where we have been able to observe it, the toxicity is characterized by hindlimb weakness and paralysis progressing rapidly over the course of one day—a sudden but rather nonspecific finding for a CNS drug, which does not in itself point to any specific mechanism. The battery of studies undertaken here illuminate several mechanistic aspects of this phenomenon.

Our data show that this phenomenon is target-independent compounds that do and do not lower *Prnp* behave similarly. Observation of similar toxicity across a wide range of ASO sequences and chemical configurations, makes it very unlikely to be driven by any specific hybridization-dependent off-target binding event. Although sequence-independent aptameric effects of phosphorothioate oligonucleotides on PrP have been

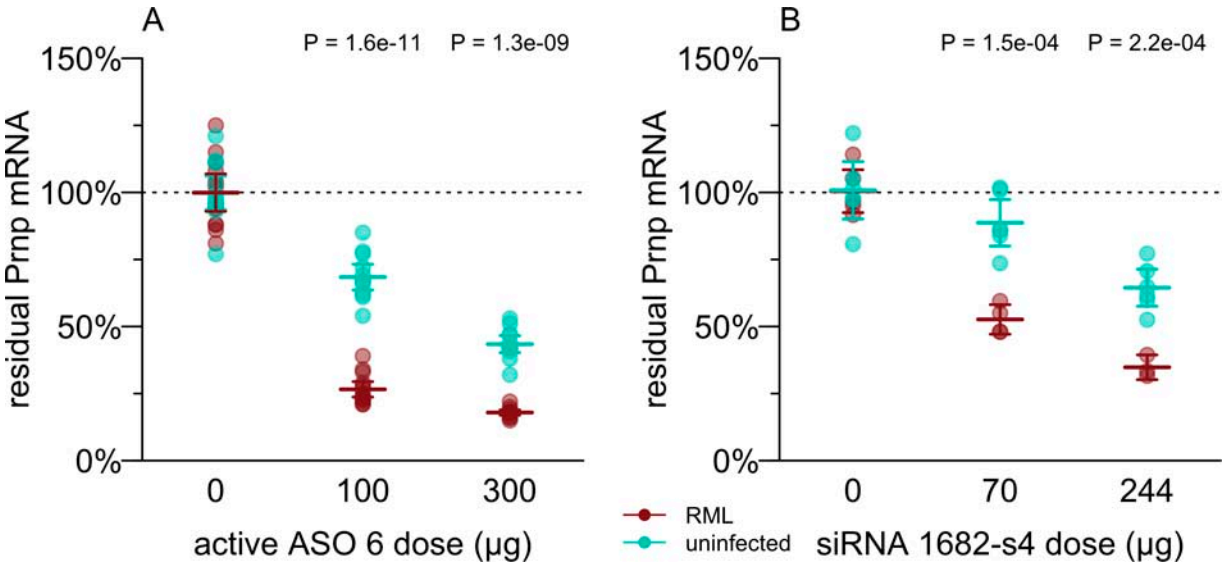


FIG. 4. Enhanced potency of two oligonucleotides in prion-infected mice. Dose-response potency studies of **(A)** ASO 6 and **(B)** divalent siRNA 1682-s4[3] in prion-infected mice. qPCR of Prnp mRNA in whole brain hemisphere; each point is one animal, segments are means and error bars are 95% confidence intervals.

reported previously, we have shown that such aptameric interactions are artifacts of the high concentrations used in biophysical experiments and are not responsible for antiprion activity in cell culture[29]; we show here that ASO binding affinities for PrP are likewise not correlated with *in vivo* toxicity. The toxicity is prion disease stage-dependent, with some ASOs showing toxicity as early as 60 dpi while others are not toxic until 123 dpi. ASOs that exhibit this prion disease-specific toxicity are not differentiated from tolerated ASOs by any inflammatory, behavioral, or histological characteristics in uninfected animals, by innate immune pathway activation, nor by pharmacokinetic uptake or tissue accumulation. The toxicity is characterized by a specific transcriptomic signature in the brain that is shared between all toxic ASOs tested, and emerges rapidly over a 7-day period post-dose. Among ASOs that were relatively better tolerated in prion-infected mice, this transcriptomic signature was absent, more muted, or appeared only transiently over 7 days but faded by 30 days post-dose. This transcriptomic signature is absent from uninfected mice receiving the same compounds, arguing that prion disease does not simply exaggerate underlying ASO toxicity. Prion disease is phenotypically heterogeneous,[43] with occasional presentations of acute decline mimicking stroke,[44–46] so we also interrogated whether ASOs might be accelerating the underlying toxicity of prion disease in our animals. We found, however, that the transcriptomic signature identified here is entirely absent from the natural history of prion disease in animals not treated with ASOs. All of the above findings argue that the toxicity is an emergent property: an interaction term between prion disease and certain ASOs. It does not represent an exacerbation of underlying ASO toxicity by prion disease, nor an exacerbation of underlying prion disease by the ASO.

In order to reach the cytosol or nucleus and become pharmacologically active, oligonucleotide therapeutics must first bind cell surface proteins, become internalized into endosomes, and then undergo endosomal escape.[47,48] Several lines of evidence led us to hypothesize that endosomal integrity may be compromised in prion disease. PrP, a GPI-anchored protein, cycles frequently through endosomal compartments,[49] and modulators of endosomal acidification can suppress prion replication in immortalized cells.[50] The spongiform holes in the brain that are pathognomonic for prion disease are in fact lysosomes engorged due to loss of PIKfyve expression.[51] Galectins—sensors of endosomal integrity used in cellular assays to monitor leakage and escape of oligonucleotides[52–54]—are upregulated in terminal prion disease.[55,56] Here, both our transcriptomic data and prior work[40] show increases in galectins 3, 9, and 3-binding protein (*Lgals3, Lgals9, Lgals3bp*) at the terminal stage. Galectin 3 (*Lgals3*) transcript expression was also somewhat increased in RML-infected animals receiving toxic ASO, but the other galectins were not significantly affected; we do not have any strong evidence that the ASO tox phenomenon involves an exacerbation of endosomal pathology. We find that both an ASO and a divalent siRNA are more potent in the prion-infected mouse brain than in uninfected animals. The magnitude of difference is large: prion infection results in 25–42 percentage points of additional target RNA knockdown at the same dose. We suspect that this may result from enhanced endosomal escape. ASO 6, the ASO used in this experiment, is generally well-tolerated in prion-infected mice, and premature deaths were never observed in prion-infected mice treated with 1682-s4, the divalent siRNA employed here.[3] Thus, deeper target engagement in the prion-infected brain is not a property specific to toxic ASOs. Rather, it may be that a range of ASOs and other oligonucleotides exhibit enhanced escape into active compartments within the prion-infected brain, but that only a subset of them are toxic under these enhanced conditions.

Our study has limitations. The battery of dosing regimens and experimental readouts examined in uninfected mice, while large, was far from exhaustive, and we may have missed discovering an assay in uninfected animals that could effectively triage which compounds are most and least likely to be toxic in prion-infected animals. In particular, we did not examine tolerability in long-term chronic dosing campaigns. Our survey of chemical configurations of ASOs was not systematic enough to reach firm mechanistic conclusions. We did observe toxicity for one fully 2'MOE modified ASO, a chemical configuration known to abolish RNase H1 cleavage, but this is not sufficient to rule in or rule out an RNase H1-dependent mechanism. Meanwhile, we observed ameliorated toxicity for one ASO with a 2'OMe modification in the gap, but this is insufficient to determine whether this holds as a general design principle. Most importantly, while we ruled out several possible explanations for prion disease-specific ASO toxicity, we were not able to pinpoint a single specific mechanism that does explain the toxicity. Indeed, while the transcriptomic signature was highly consistent across toxic ASOs and is highly enriched for downregulated astrocyte transcripts, we were unable to determine what property these transcripts have in common or what, mechanistically, they may signify.

Our data establish that the ASO toxicity phenomenon in prion disease mice is a specific and reproducible interaction between ASO and prion disease, rather than an exacerbation of one by the other, and is shared across a variety of different ASOs, regardless of molecular target, but only at high doses and at sufficiently advanced disease stages.

Data Availability

Raw data and source code sufficient to reproduce figures and statistics in this article are available at github.com/vallabhminikel/toxseq.

Author Disclosure Statement

E.V.M. has received speaking fees from AbbVie, Eli Lilly, Novartis, Vertex, and Voyager; consulting fees from Alnylam, Arrowhead, Deerfield, and Regeneron; and research support from Cenos, Eli Lilly, Gate Bio, Ionis, Regeneron, and Sangamo Therapeutics. S.M.V. acknowledges speaking fees from Abbvie, Biogen, Eli Lilly, Illumina, Ultragenyx, and Voyager; consulting fees from Alnylam, Invitae, and Regeneron; research support from Cenos, Eli Lilly, Gate Bio, Ionis, Regeneron, and Sangamo Therapeutics. H.T.Z., S.D., B.N., H.L., J.M., Susan L., S.K., and H.B.K. are employees and shareholders of Ionis Pharmaceuticals.

Funding Information

This work was supported by the National Institutes of Health (R01 NS125255 to SMV and P20 GM152335 to AGP), by the Next Gen Fund at the Broad Institute, and by Ionis Pharmaceuticals. Colony management and animal

procedures were performed by the Weissman Hood Institute at Touro University; McLaughlin Research Institute Gene Editing and Mouse Models Assessment Core Facility within the Center for Integrated Biomedical and Rural Health Research, RRID:SCR_027045, P20 GM152335.

Supplementary Material

Supplementary Data

References

1. Raymond GJ, Zhao HT, Race B, et al. Antisense oligonucleotides extend survival of prion-infected mice. JCI Insight 2019;5:e131175; doi: 10.1172/jci.insight.131175
2. Minikel EV, Zhao HT, Le J, et al. Prion protein lowering is a disease-modifying therapy across prion disease stages, strains and endpoints. Nucleic Acids Res 2020;48:10615–10631; doi: 10.1093/nar/gkaa616
3. Gentile JE, Corridon TL, Serack FE, et al. Divalent siRNA for prion disease. Nucleic Acids Res 2026;54:gkag287; doi: 10.1093/nar/gkag287
4. Nazor Friberg K, Hung G, Wancewicz E, et al. Intracerebral infusion of antisense oligonucleotides into prion-infected mice. Mol Ther Nucleic Acids 2012;1:e9; doi: 10.1038/mtna.2011.6
5. Shen W, De Hoyos CL, Migawa MT, et al. Chemical modification of PS-ASO therapeutics reduces cellular protein-binding and improves the therapeutic index. Nat Biotechnol 2019;37:640–650; doi: 10.1038/s41587-019-0106-2
6. Burel SA, Hart CE, Cauntay P, et al. Hepatotoxicity of high affinity gapmer antisense oligonucleotides is mediated by RNase H1 dependent promiscuous reduction of very long pre-mRNA transcripts. Nucleic Acids Res 2016;44:2093–2109; doi: 10.1093/nar/gkv1210
7. Kamola PJ, Kitson JDA, Turner G, et al. In silico and *in vitro* evaluation of exonic and intronic off-target effects form a critical element of therapeutic ASO gapmer optimization. Nucleic Acids Res 2015;43:8638–8650; doi: 10.1093/nar/gkv857
8. Kasuya T, Hori S-I, Watanabe A, et al. Ribonuclease H1-dependent hepatotoxicity caused by locked nucleic acid-modified gapmer antisense oligonucleotides. Sci Rep 2016;6:30377; doi: 10.1038/srep30377
9. Kakiuchi-Kiyota S, Koza-Taylor PH, Mantena SR, et al. Comparison of hepatic transcription profiles of locked ribonucleic acid antisense oligonucleotides: Evidence of distinct pathways contributing to non-target mediated toxicity in mice. Toxicol Sci 2014;138:234–248; doi: 10.1093/toxsci/kft278
10. Hagedorn PH, Yakimov V, Ottosen S, et al. Hepatotoxic potential of therapeutic oligonucleotides can be predicted from their sequence and modification pattern. Nucleic Acid Ther 2013;23:302–310; doi: 10.1089/nat.2013.0436
11. Burdick AD, Sciabola S, Mantena SR, et al. Sequence motifs associated with hepatotoxicity of locked nucleic acid–modified antisense oligonucleotides. Nucleic Acids Res 2014;42:4882–4891; doi: 10.1093/nar/gku142
12. Hagedorn PH, Brown JM, Easton A, et al. Acute neurotoxicity of antisense oligonucleotides after intracerebroventricular injection into mouse brain can be predicted from sequence features. Nucleic Acid Ther 2022;32:151–162; doi: 10.1089/nat.2021.0071
13. O'Rourke JG, Bachmann G, Mazur C, et al. Acute neuronal inhibition response caused by phosphorothioate antisense oligonucleotides following local delivery to the central nervous system. Nucleic Acids Res 2026;54:gkaf1333; doi: 10.1093/nar/gkaf1333
14. Moazami MP, Rembetsy-Brown JM, Sarli SL, et al. Quantifying and mitigating motor phenotypes induced by antisense oligonucleotides in the central nervous system. Mol Ther 2024;32:4401–4417; doi: 10.1016/j.ymthe.2024.10.024
15. Bravo-Hernandez M, Mazur C, Chen H, et al. Transient acute neuronal activation response caused by high concentrations of oligonucleotides in the cerebral spinal fluid. Nucleic Acids Res 2026;54:gkag057; doi: 10.1093/nar/gkag057
16. Jia C, Lei Mon SS, Yang Y, et al. Change of intracellular calcium level causes acute neurotoxicity by antisense oligonucleotides via CSF route. Mol Ther Nucleic Acids 2023;31:182–196; doi: 10.1016/j.omtn.2022.12.010
17. Miller R, Paquette J, Barker A, et al. Preventing acute neurotoxicity of CNS therapeutic oligonucleotides with the addition of Ca2+ and Mg2+ in the formulation. Mol Ther Nucleic Acids 2024;35:102359; doi: 10.1016/j.omtn.2024.102359
18. Hagemann TL, Connor JX, Messing A. Alexander disease-associated glial fibrillary acidic protein mutations in mice induce Rosenthal fiber formation and a white matter stress response. J Neurosci 2006;26:11162–11173; doi: 10.1523/JNEUROSCI.3260-06.2006
19. Chandler RL. Encephalopathy in mice produced by inoculation with scrapie brain material. Lancet 1961;1:1378–1379.
20. Jafar-Nejad P, Powers B, Soriano A, et al. The atlas of RNase H antisense oligonucleotide distribution and activity in the CNS of rodents and non-human primates following central administration. Nucleic Acids Res 2021;49:657–673; doi: 10.1093/nar/gkaa1235
21. Mazur C, Fitzsimmons B, Kamme F, et al. Development of a simple, rapid, and robust intrathecal catheterization method in the rat. J Neurosci Methods 2017;280:36–46; doi: 10.1016/j.jneumeth.2017.02.001
22. Kordasiewicz HB, Stanek LM, Wancewicz EV, et al. Sustained therapeutic reversal of Huntington's disease by transient repression of huntingtin synthesis. Neuron 2012;74:1031–1044; doi: 10.1016/j.neuron.2012.05.009
23. Pollak AJ, Cauntay P, Machemer T, et al. Inflammatory Non-CpG antisense oligonucleotides are signaling through TLR9 in human burkitt lymphoma B Bjab cells. Nucleic Acid Ther 2022;32:473–485; doi: 10.1089/nat.2022.0034
24. Yu RZ, Graham MJ, Post N, et al. Disposition and pharmacology of a GalNAc3-conjugated ASO targeting human lipoprotein (a) in mice. Mol Ther Nucleic Acids 2016;5:e317; doi: 10.1038/mtna.2016.26
25. Damle SS, Watt A, Kuntz S, et al. A workflow for transcriptome-wide assessment of antisense oligonucleotide selectivity. Nucleic Acid Ther 2025;35:249–260; doi: 10.1177/21593337251378141
26. Patro R, Duggal G, Love MI, et al. Salmon provides fast and bias-aware quantification of transcript expression. Nat Methods 2017;14:417–419; doi: 10.1038/nmeth.4197
27. Love MI, Huber W, Anders S. Moderated estimation of fold change and dispersion for RNA-seq data with DESeq2. Genome Biol 2014;15:550; doi: 10.1186/s13059-014-0550-8
28. Mortberg MA, Gentile JE, Nadaf NM, et al. A single-cell map of antisense oligonucleotide activity in the brain. Nucleic Acids Res 2023;51:7109–7124; doi: 10.1093/nar/gkad371
29. Reidenbach AG, Minikel EV, Zhao HT, et al. Characterization of the prion protein binding properties of antisense

oligonucleotides. Biomolecules 2019;10:1; doi: 10.3390/biom10010001
30. Freier SM. Compounds and Methods for Reducing LRRK2 Expression. World Intellectual Property Organization: Geneva, Switzerland; 2025. Available from: https://patents.google.com/patent/WO2020006267A1/en
31. Minikel EV. Rationale for Early Therapeutic Intervention in Genetic Prion Disease. PhD Dissertation. Harvard University: Cambridge, MA; 2019.
32. Tamgüney G, Francis KP, Giles K, et al. Measuring prions by bioluminescence imaging. Proc Natl Acad Sci U S A 2009;106:15002–15006; doi: 10.1073/pnas.0907339106
33. Bridel C, van Wieringen WN, Zetterberg H, et al.; and the NFL Group. Diagnostic value of cerebrospinal fluid neurofilament light protein in neurology: A systematic review and meta-analysis. JAMA Neurol 2019;76:1035–1048; doi: 10.1001/jamaneurol.2019.1534
34. McInnes L, Healy J, Melville J. UMAP: Uniform Manifold Approximation and Projection for Dimension Reduction. ArXiv 2018; doi: 10.48550/ARXIV.1802.03426
35. Fazal FM, Han S, Parker KR, et al. Atlas of subcellular RNA localization revealed by APEX-Seq. Cell 2019;178:473–490.e26; doi: 10.1016/j.cell.2019.05.027
36. Engel KL, Lo H-YG, Goering R, et al. Analysis of subcellular transcriptomes by RNA proximity labeling with Halo-seq. Nucleic Acids Res 2022;50:e24; doi: 10.1093/nar/gkab1185
37. Nakaya T, Maragkakis M. Amyotrophic lateral sclerosis associated FUS mutation shortens mitochondria and induces neurotoxicity. Sci Rep 2018;8:15575; doi: 10.1038/s41598-018-33964-0
38. Subramanian A, Tamayo P, Mootha VK, et al. Gene set enrichment analysis: A knowledge-based approach for interpreting genome-wide expression profiles. Proc Natl Acad Sci U S A 2005;102:15545–15550; doi: 10.1073/pnas.0506580102
39. Anderson BA, Freestone GC, Low A, et al. Towards next generation antisense oligonucleotides: Mesylphosphoramidate modification improves therapeutic index and duration of effect of gapmer antisense oligonucleotides. Nucleic Acids Res 2021;49:9026–9041; doi: 10.1093/nar/gkab718
40. Sorce S, Nuvolone M, Russo G, et al. Genome-wide transcriptomics identifies an early preclinical signature of prion infection. PLoS Pathog 2020;16:e1008653; doi: 10.1371/journal.ppat.1008653
41. Corridon TL, O'Moore J, Seerley A, et al. PrP turnover *in vivo* and the time to effect of prion disease therapeutics. PLoS Pathog 2026;22:e1014263; doi: 10.1371/journal.ppat.1014263
42. Mortberg MA, et al. PrP dosage controls prion disease tempo across myriad model systems. In Preparation. n.d.
43. Baiardi S, Capellari S, Bartoletti Stella A, et al. Unusual clinical presentations challenging the early clinical diagnosis of Creutzfeldt-jakob disease. J Alzheimers Dis 2018;64:1051–1065; doi: 10.3233/JAD-180123
44. Sharma DK, Boggild M, van Heuven AW, et al. Creutzfeldt-jakob disease presenting as stroke: A case report and systematic literature review. Neurologist 2017;22:48–53; doi: 10.1097/NRL.0000000000000107
45. Okamoto K, Abe T, Itoh Y. A case of Creutzfeldt-Jakob disease with stroke-like onset. J Stroke Cerebrovasc Dis 2020;29:104788; doi: 10.1016/j.jstrokecerebrovasdis.2020.104788
46. Balash Y, Korczyn AD, Khmelev N, et al. Creutzfeldt-jakob and vascular brain diseases: Their overlap and relationships. Front Neurol 2021;12:613991; doi: 10.3389/fneur.2021.613991
47. Crooke ST, Wang S, Vickers TA, et al. Cellular uptake and trafficking of antisense oligonucleotides. Nat Biotechnol 2017;35:230–237; doi: 10.1038/nbt.3779
48. Dowdy SF. Endosomal escape of RNA therapeutics: How do we solve this rate-limiting problem? RNA 2023;29:396–401; doi: 10.1261/rna.079507.122
49. Harris DA, Huber MT, van Dijken P, et al. Processing of a cellular prion protein: Identification of N- and C-terminal cleavage sites. Biochemistry 1993;32:1009–1016.
50. Doh-Ura K, Iwaki T, Caughey B. Lysosomotropic agents and cysteine protease inhibitors inhibit scrapie-associated prion protein accumulation. J Virol 2000;74:4894–4897.
51. Lakkaraju AKK, Frontzek K, Lemes E, et al. Loss of PIKfyve drives the spongiform degeneration in prion diseases. EMBO Mol Med 2021;13:e14714; doi: 10.15252/emmm.202114714
52. Aits S, Kricker J, Liu B, et al. Sensitive detection of lysosomal membrane permeabilization by lysosomal galectin puncta assay. Autophagy 2015;11:1408–1424; doi: 10.1080/15548627.2015.1063871
53. Du Rietz H, Hedlund H, Wilhelmson S, et al. Imaging small molecule-induced endosomal escape of siRNA. Nat Commun 2020;11:1809; doi: 10.1038/s41467-020-15300-1
54. Munson MJ, O'Driscoll G, Silva AM, et al. A high-throughput Galectin-9 imaging assay for quantifying nanoparticle uptake, endosomal escape and functional RNA delivery. Commun Biol 2021;4:211; doi: 10.1038/s42003-021-01728-8
55. Mok SWF, Riemer C, Madela K, et al. Role of galectin-3 in prion infections of the CNS. Biochem Biophys Res Commun 2007;359:672–678; doi: 10.1016/j.bbrc.2007.05.163
56. Makarava N, Safadi T, Pandit NP, et al. Protective role of galectin-3 in prion disease through regulation of microglial PrP^{Sc} uptake. bioRxiv 2026; doi: 10.64898/2026.06.11.731738

Address correspondence to:
Eric Vallabh Minikel, PhD
Program in Brain Health
Broad Institute of MIT and Harvard
415 Main St
Cambridge, MA 024142
USA

E-mail: eminikel@broadinstitute.org

Received for publication July 24, 2026; accepted after revision September 19, 2026; Published Online: Month 00, 2026.

Supplement

treatment	same-day deaths	four-week deaths	days post-treatment
saline	—	2/6	12-17
active ASO 1	—	2/6	9
control ASO 3	—	5/6	9-18
control ASO 4	—	1/6	22
active ASO 5	—	2/5	22
active ASO 6	—	1/6	12
active ASO 7	—	5/6	6-7
active ASO 8	3/6	3/3	6-7

Table S1. Four-week tolerability testing of ASOs in prion-infected mice at 120 dpi. *Studies conducted at the Broad Institute in wild-type C57BL/6N mice intracerebrally infected with RML prions and treated with a single 500 μg ICV dose. Active ASO 2 was not evaluated in this study due to an insufficient number of animals available for dividing into treatment groups. Active ASO 8 caused acute death (within hours of surgery) in 3/6 mice. In each of the remaining treatment groups, including the saline group, all mice survived the day of surgery but some died or became acutely sick within a few weeks. Of animals that died within the four-week window (N=21 total), most were either euthanized upon advanced but non-specific neurological signs (N=11), or were found dead (N=7). In a few animals (N=3, one each from active ASOs 5, 7, and 8), hindlimb paralysis was noted to develop rapidly over the course of approximately 24 hours. Complications of prion disease or of ICV surgery are also possible explanations for some deaths in this time period, however, and two saline-treated animals also succumbed — one was euthanized with sudden neurological signs at 12 days post-surgery and one was found dead at 17 days post-surgery. These data were previously included in a dissertation[32].*

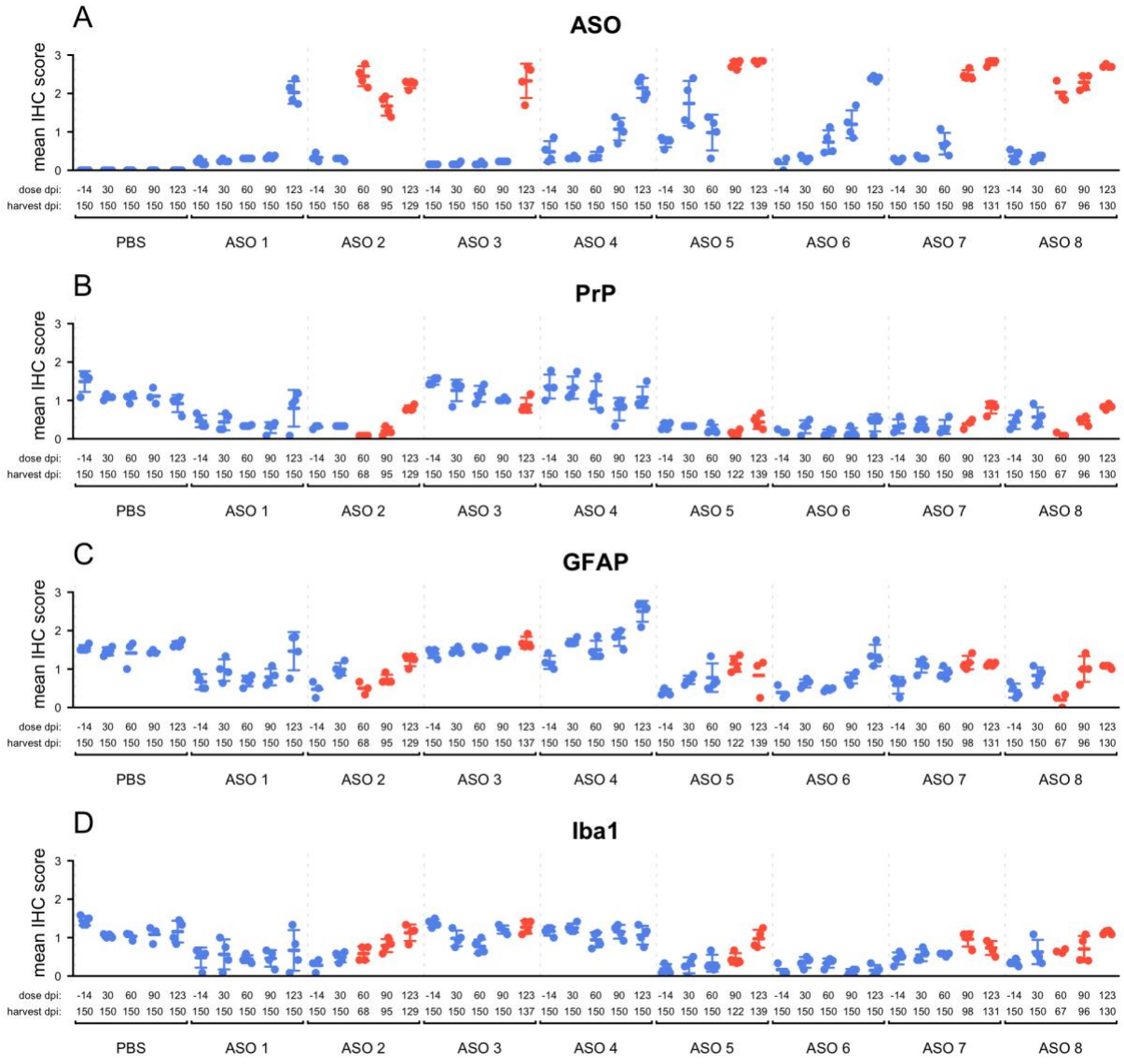


Figure S1. Brain histology analysis of RML-infected mice receiving toxic or tolerated ASOs. *Animals from the time-series study depicted in Figure 1B were dosed with ASO, and harvested for histology analysis, at the respective timepoints listed along the x axis of every panel. ASO/timepoint combinations that were tolerated are shown in blue, and toxic in orange.* ***A)*** *ASO, stained with an antibody to the phosphorothioate backbone. Note that toxic ASO animals were necessarily harvested much sooner post-dose than tolerated ASO animals, hence their brain ASO concentration is much higher.* ***B)*** *PrP. Note that ASOs 1, 2, 5, 6, 7, and 8 are all PrP-lowering, while ASOs 3 and 4 are non-targeting controls.* ***C)*** *GFAP, and* ***D)*** *Iba1.*

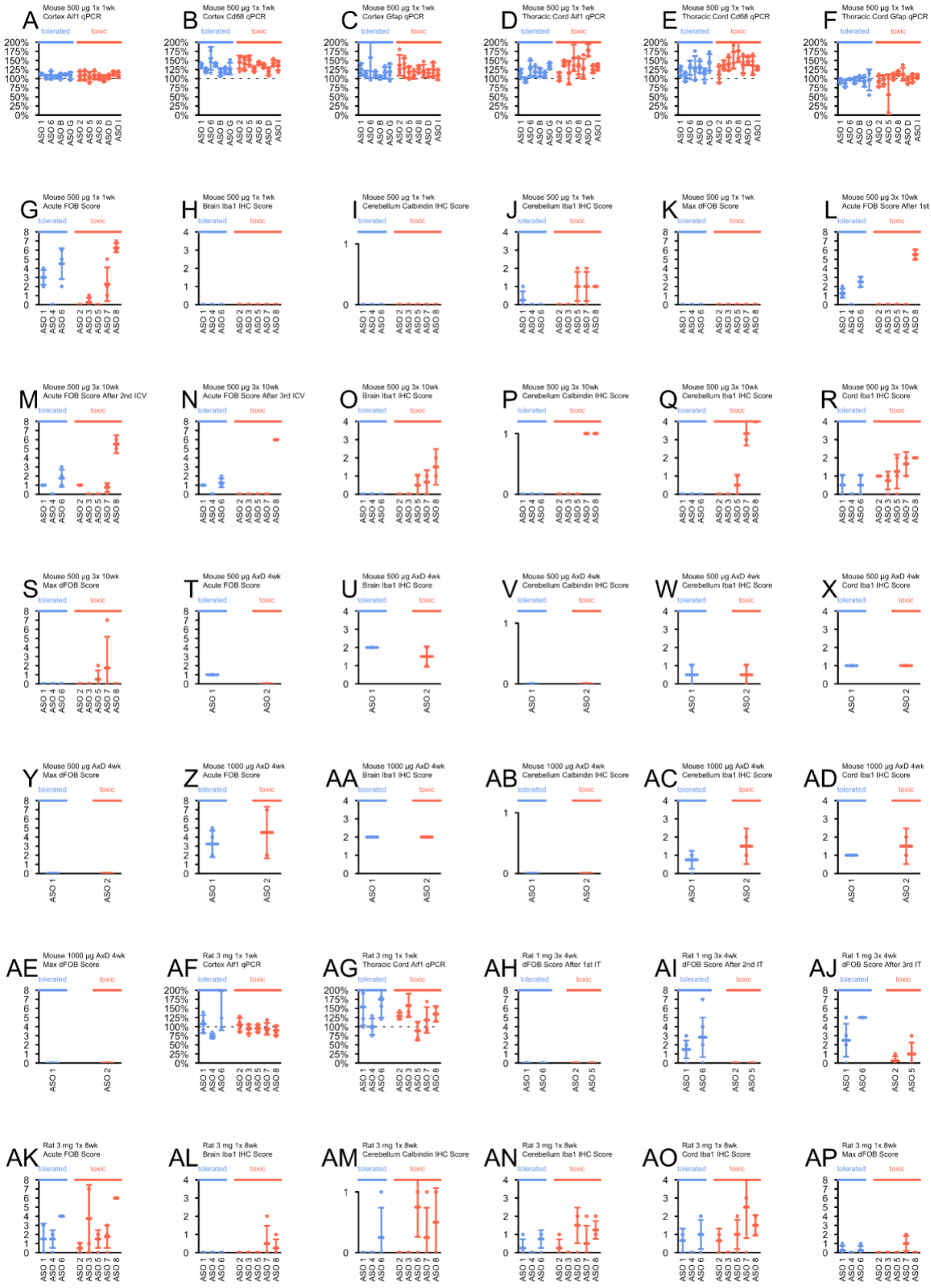

A
Mouse 500 µg 1x 1wk
Cortex Aif1 qPCR
B
Mouse 500 µg 1x 1wk
Cortex Cd68 qPCR
C
Mouse 500 µg 1x 1wk
Cortex Gfap qPCR
D
Mouse 500 µg 1x 1wk
Thoracic Cord Aif1 qPCR
E
Mouse 500 µg 1x 1wk
Thoracic Cord Cd68 qPCR
F
Mouse 500 µg 1x 1wk
Thoracic Cord Gfap qPCR
G
Mouse 500 µg 1x 1wk
Acute FOB Score
H
Mouse 500 µg 1x 1wk
Brain Iba1 IHC Score
I
Mouse 500 µg 1x 1wk
Cerebellum Calbindin IHC Score
J
Mouse 500 µg 1x 1wk
Cerebellum Iba1 IHC Score
K
Mouse 500 µg 1x 1wk
Max dFOB Score
L
Mouse 500 µg 3x 10wk
Acute FOB Score After 1st ICV
M
Mouse 500 µg 3x 10wk
Acute FOB Score After 2nd ICV
N
Mouse 500 µg 3x 10wk
Acute FOB Score After 3rd ICV
O
Mouse 500 µg 3x 10wk
Brain Iba1 IHC Score
P
Mouse 500 µg 3x 10wk
Cerebellum Calbindin IHC Score
Q
Mouse 500 µg 3x 10wk
Cerebellum Iba1 IHC Score
R
Mouse 500 µg 3x 10wk
Cord Iba1 IHC Score
S
Mouse 500 µg 3x 10wk
Max dFOB Score
T
Mouse 500 µg AxD 4wk
Acute FOB Score
U
Mouse 500 µg AxD 4wk
Brain Iba1 IHC Score
V
Mouse 500 µg AxD 4wk
Cerebellum Calbindin IHC Score
W
Mouse 500 µg AxD 4wk
Cerebellum Iba1 IHC Score
X
Mouse 500 µg AxD 4wk
Cord Iba1 IHC Score
Y
Mouse 500 µg AxD 4wk
Max dFOB Score
Z
Mouse 1000 µg AxD 4wk
Acute FOB Score
AA
Mouse 1000 µg AxD 4wk
Brain Iba1 IHC Score
AB
Mouse 1000 µg AxD 4wk
Cerebellum Calbindin IHC Score
AC
Mouse 1000 µg AxD 4wk
Cerebellum Iba1 IHC Score
AD
Mouse 1000 µg AxD 4wk
Cord Iba1 IHC Score
AE
Mouse 1000 µg AxD 4wk
Max dFOB Score
AF
Rat 3 mg 1x 1wk
Cortex Aif1 qPCR
AG
Rat 3 mg 1x 1wk
Thoracic Cord Aif1 qPCR
AH
Rat 1 mg 3x 4wk
dFOB Score After 1st IT
AI
Rat 1 mg 3x 4wk
dFOB Score After 2nd IT
AJ
Rat 1 mg 3x 4wk
dFOB Score After 3rd IT
AK
Rat 3 mg 1x 8wk
Acute FOB Score
AL
Rat 3 mg 1x 8wk
Brain Iba1 IHC Score
AM
Rat 3 mg 1x 8wk
Cerebellum Calbindin IHC Score
AN
Rat 3 mg 1x 8wk
Cerebellum Iba1 IHC Score
AO
Rat 3 mg 1x 8wk
Cord Iba1 IHC Score
AP
Rat 3 mg 1x 8wk
Max dFOB Score
tolerated
toxic

Figure S2. Additional endpoints examined in naive mice and rats. *Each panel represents one inflammatory, immunohistochemical, or behavioral endpoint evaluated in one experiment in uninfected mice or rats. Experimental paradigm abbreviations are as follows. Mouse 500 µg 1x 1wk: mice received a single 500 µg ICV dose and were harvested 1 week later. Mouse 500 µg 3x 10wk: mice received 500 µg ICV doses at week 0, 1, 2, and were harvested at week 10. Mouse 500 µg AxD 4wk: Alexander disease (AxD) mice*[18] *received 500 µg ICV doses at week 0 and were harvested at week 4. Mouse 1000 µg AxD 4wk: Alexander disease (AxD) mice*[18] *received 1000 µg ICV doses at week 0 and were harvested at week 4. Rat 3mg 1x 1wk: rats received 3 mg IT doses at week 0 and were harvested at week 1. Rat 1mg 3x 4wk: rats received 1 mg IT doses at week 0, 1, 2, and were harvested at week 4. Rat 3mg 1x 8wk: rats received 3 mg IT doses at week 0 and were harvested at week 8. Endpoints descriptions are provided in the Methods.*

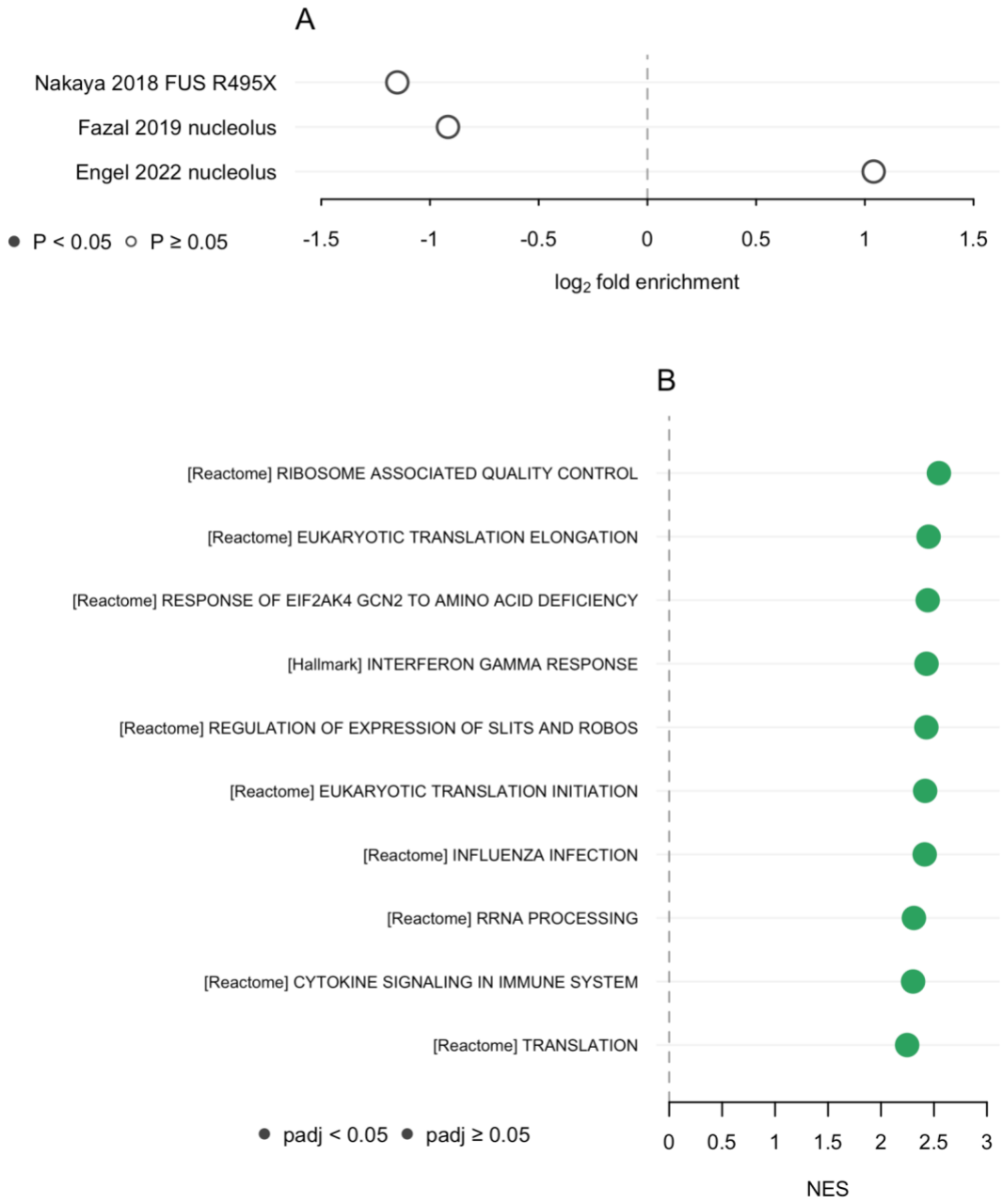


Figure S3. Gene set and pathway enrichment analyses. *For all analyses, the 65 genes identified in the toxic ASO signature were used as the test set.* ***A)*** *Gene set enrichment analyses using a hypergeometric test: genes downregulated upon expression of FUS R495X in neuronally differentiated mouse embryonic stem cells (Nakaya 2018 Table S6)[38]; nucleolar genes from an APEX-seq atlas (Fazal 2019 Table S3)[36], and nucleolar genes identified by Halo-seq using a Halo-fibrillarin fusion (Engel 2022 Table S3)[37].* ***B)*** *Gene set enrichment analyses using gene sets from Reactome, Hallmark, and GOBP, analyzed using GSEA[39].*

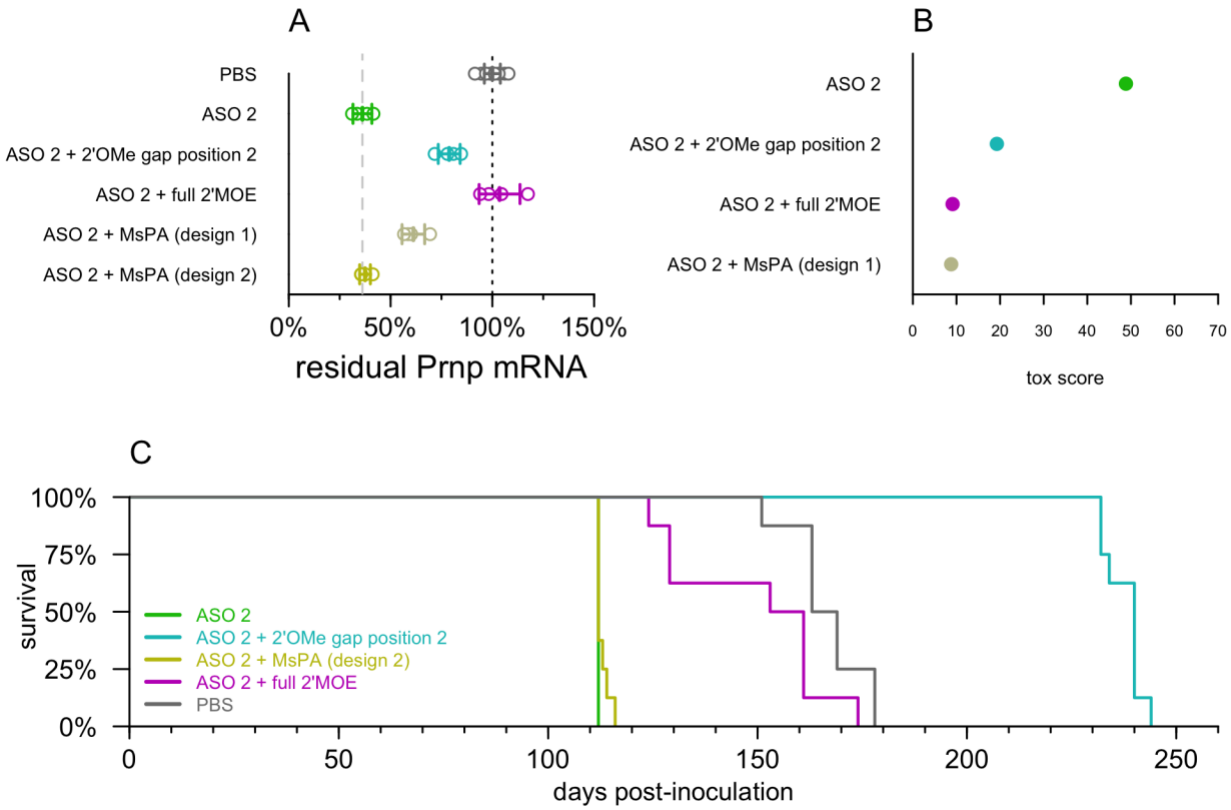


Figure S4. Evaluation of gap modifications of toxic ASO 2. A) *Potency of modified variants of ASO 2 in mouse cortex 14 days after a single 300 µg ICV dose by qPCR.* ***B)*** *Tox scores for ASO 2 and modified variants administered to RML prion-infected mice at 300 µg ICV at 120 dpi with brain harvest at 127 dpi, 7 days post-dose.* ***C)*** *Survival of RML prion-infected mice receiving a single 300 µg ICV dose of ASO 2 or modified variants at 105 dpi. PBS-treated animals died at a median of 166 dpi, consistent with the natural history of RML prion infection (Figure 1C and ref 2). 8/8 animals that received parent ASO 2 died at exactly 7 days-post dose, and 8/8 receiving the MsPA design 2 variant died between 7-11 days post dose. The full 2'MOE compound, which is inactive against Prnp and was not expected to increase survival, decreased survival slightly but significantly to a median of 157 dpi (P = 0.023, 2-sided pairwise log-rank test vs. PBS). The variant with 2'OMe at gap position 2 proved tolerated and efficacious, with 8/8 animals outliving the last PBS animal, for a median survival of 240 dpi (+45% survival time, P = 6.2e-5, 2-sided pairwise log-rank test vs. PBS).*

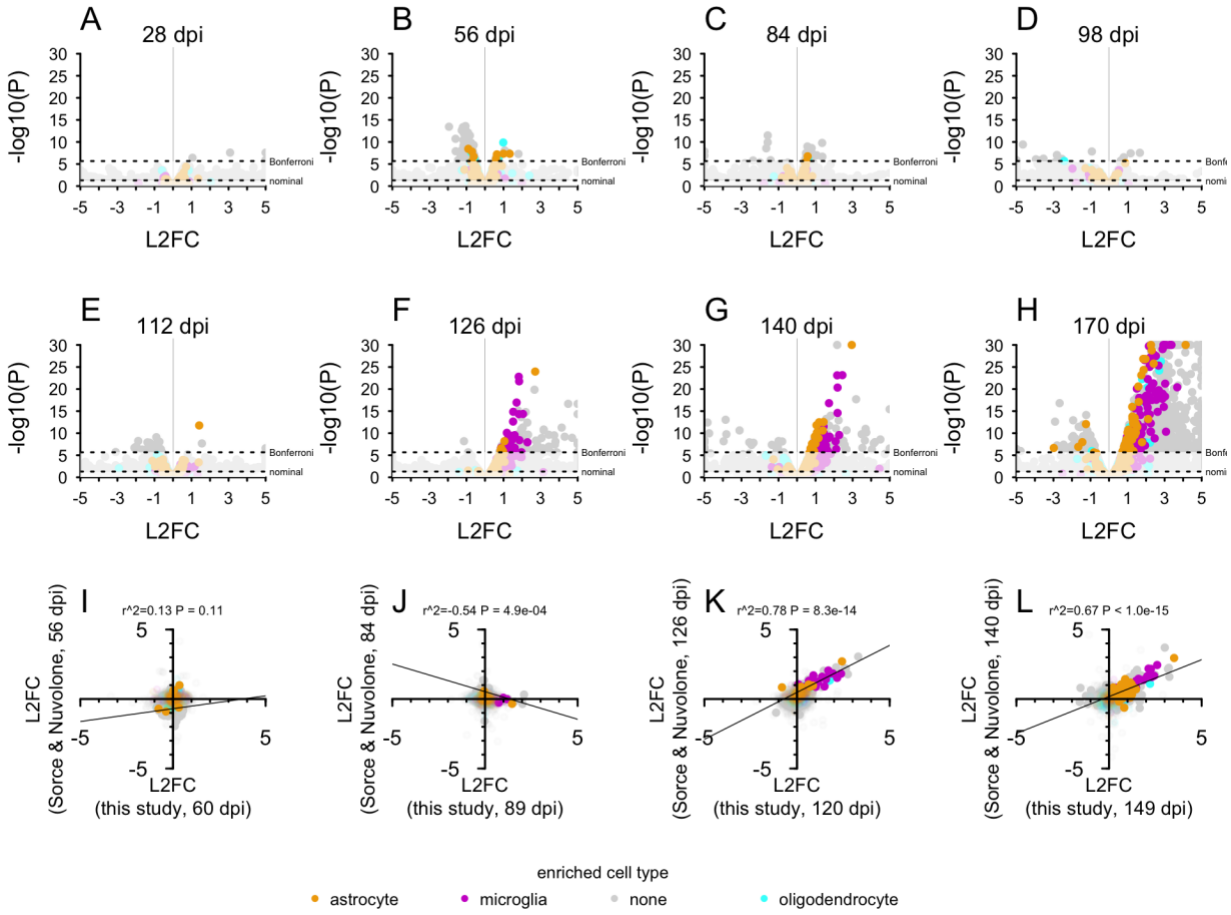


Figure S5. The transcriptomic signature of RML prion disease progression in mice. A-H) *Volcano plots of RNA-seq data from Sorce & Nuvolone 2020[41] supplementary table 2, re-plotted in our style. The x axis is log2 fold change, capped at a range of [-5,5] and the y axis is -log10 of the nominal P value, capped at a range of [0, 30]. The cutoffs for nominal (P=0.05) and Bonferroni-corrected significance are shown.* ***I-L)*** *Comparisons of the log2 fold changes in our time series transcriptomic data (same data as Figure 3; x axis) versus the nearest timepoints from the Sorce & Nuvolone dataset (y axis). Each point is one gene. Genes that are significant after multiple testing correction in either dataset are shown in full opacity, while those that are non-significant in both datasets are shown partially transparent. The r^2 and P value at top are Pearson's correlations, and the best fit line shown is a linear regression.*

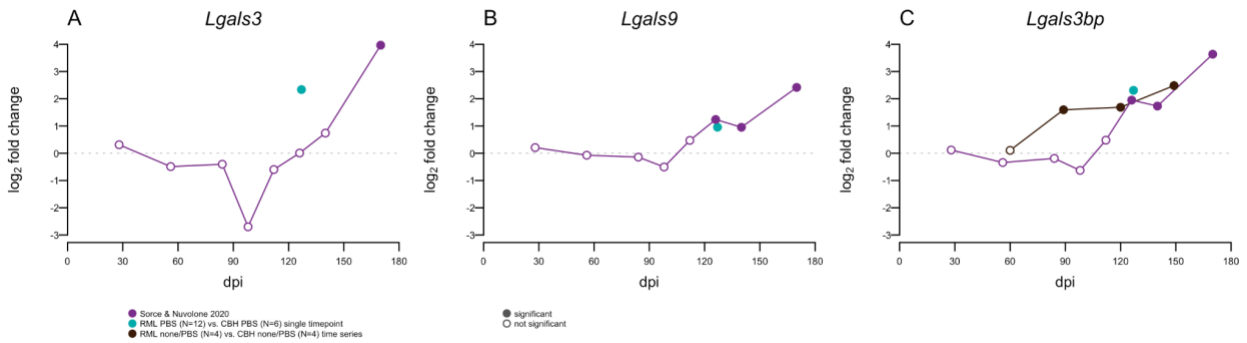


Figure S6. Temporal trajectories of galectin genes in transcriptomic datasets in RML prion infection. A) *Lgals3,* ***B)*** *Lgals9, and* ***C)*** *Lgals3bp. The x axis is days post-inoculation, the y axis is log2 fold change. Hollow symbols have P values non-significant after multiple testing correction, while solid symbols are significant after multiple testing correction. Different datasets are shown in different colors as indicated.*